

# The Detection of Opacification on the Posterior Capsule by Texture-based Segmentation

M. Holden

Department of Physics,  
King's College London,  
University of London

## Abstract

*As part of a study on the cataracts eye disorder investigations on how to automatically quantify the extent of the associated opacification were carried out. Some 169 digital images of the eyes of patient's fitted with an artificial lens were systematically analysed. Observations made of these images led to the identification of four distinct textural region classes. From an analysis of the differences in textural properties of these region classes a set of feature extractors were proposed and validated experimentally. A feature vector extractor algorithm was developed that from a set of example sub-image region classes generated a set of patterns in 4D feature space. The patterns were then classified with a multi-layer perceptron back propagation neural network. Preliminary results on data not used in training indicated a 100 percent classification accuracy for 800 pixels extracted from clear regions and a 99 percent classification accuracy for 800 pixels extracted from opacified ones.*

# Contents

<b>1</b>	<b>INTRODUCTION</b>	<b>2</b>
<b>2</b>	<b>DESCRIPTION OF THE CLINICAL CONDITION AND IM- AGERY</b>	<b>2</b>
2.1	Clinical Condition and Treatment . . . . .	2
2.2	Image Capture, Storage and Identification . . . . .	3
2.3	Description of Imagery . . . . .	4
2.4	Visual Classification of Image Regions . . . . .	4
<b>3</b>	<b>ANALYSIS OF THE IMAGERY</b>	<b>6</b>
3.1	Assessment of Software Tools . . . . .	6
3.2	Reference Images . . . . .	7
3.3	Noise in Images . . . . .	7
3.4	Locating the Area of Interest . . . . .	8
3.5	General Statistical Properties of the Images . . . . .	9
3.6	Texture Characterisation of Image Region Classes . . . . .	12
3.7	Feature Extractors . . . . .	12
<b>4</b>	<b>THE FEATURE VECTOR EXTRACTOR</b>	<b>17</b>
4.1	Software Requirements . . . . .	18
4.2	Software Design and Implementation . . . . .	19
4.3	Data Organisation . . . . .	19
4.4	The Feature Vector Extractor Algorithm . . . . .	19
<b>5</b>	<b>FEATURE CLASSIFICATION</b>	<b>20</b>
5.1	Training and Validation Data Sets . . . . .	22
5.2	Experiments with the Pattern Classifier . . . . .	23
5.3	Selecting an Architecture and Weights (Training) . . . . .	24
<b>6</b>	<b>RESULTS</b>	<b>25</b>
<b>7</b>	<b>CONCLUSIONS</b>	<b>25</b>
<b>8</b>	<b>FURTHER WORK</b>	<b>26</b>

# 1 INTRODUCTION

Automatically aided diagnosis is an important research area in medical image processing. The work presented here has been carried out as part of collaborative research programme between the Department of Ophthalmology, St Thomas's Hospital and the Department of Physics, King's College. A major research goal is the provision of tools for the automatic detection of eye disorders, in particular opacified areas of a cataractous eye. The objective of this investigation is to establish how the relative areas of normal and opacified tissue in a cataractous eye could be quantified. Since the medical diagnosis of cataracts is made by human expert judgement it is necessarily subject to some human error. A target error bound of 10% has therefore been established as a realistic aim. The approach taken started with a study of the clinical condition and the method of image capture followed by a detailed descriptive summary of the available data. Then the noise and statistical properties of examples of the imagery were investigated. From these properties and other observations four different textural region classes were identified. Analysis of the textural properties of the region classes led to the proposal of a set of candidate feature extractors (operators) different to those used in earlier related work [1]. The suitability of each feature extractor (operator) was assessed experimentally. On the basis of the experimental results four of these operators were selected and incorporated into a feature vector extractor algorithm. A set of exemplar sub-images of the region classes were then extracted from the data set. To facilitate their storage and subsequent retrieval a simple storage scheme was formulated. The feature vector extractor was applied to the exemplar set of sub-images to generate a set of training patterns (one per pixel) which was used by a multi-layer perceptron (MLP) neural network to derive a decision boundary in 4D feature space. The MLP was then used to classify sub-regions of a different image to the ones used during training. The work was carried out using a decstation 5000/133 with MIPS R3000 processor, 32 M Bytes of RAM, 50 M Bytes of swap-space, the ULTRIX OS, X-windows, the Khoros image processing package and an MLP algorithm developed by the Department of Physics, King's College.

## 2 DESCRIPTION OF THE CLINICAL CONDITION AND IMAGERY

### 2.1 Clinical Condition and Treatment

Patients with cataracts often require surgery as part of their medical treatment. A common surgical procedure taken involves the following steps [2]: (1) making an incision in the outside of the eye such as the cornea; (2) making an incision in the anterior capsule; (3) removing the cataractous lens; (4) inserting a plastic intraocular lens (IOL) into the capsular bag through the hole in the anterior capsule (capsulorrhexis); (5) sealing the wound in the outside of the eye. Three different types of IOLs were used, fabricated from different materials and utilising different types of haptics (lens holders). Unfortunately, the operation is

not one hundred percent successful because, in some cases, of the recurrence of an opacification on the posterior capsule [3]. The recurrence appears to be a result of two main processes: Physical, due to: (a) the rotational movement of capsule which can cause the edges of the incision to obstruct the field of view. Biological, due to: (b) the contraction of the fibrous cells (thought to be the result of movements of the capsule) which results in surface folds; (c) the growth of cellular membrane tissue on the posterior lens' surface; (d) the growth of fibrous strands.

As part of the study some 90 patients were asked to attend a series of appointments at intervals of 1, 3, 6 and 12 months following their operation. During each appointment a digital image of the affected eye was captured and used to provide a record of the condition of the patient's eye during the study period. Unfortunately, due to ill health and other factors, not all patients attended every appointment, consequently the data set is incomplete. Images captured during months 1 and 3 were available for analysis, 169 images in total, 85 for month 1 and 84 for month 3. Nine month 1 images have no corresponding one in month 3, and eight month 3 images do not have a corresponding one in month 1. There are, therefore, 76 common images in the records for months 1 and 3.

## 2.2 Image Capture, Storage and Identification

Images were captured with a Zeiss anterior segment photo-slit lamp with an added beam-splitter that provides retro-illuminated images. Retro-illumination involves directing a beam of light into the eye and observing the reflections from the surface of the retina (c.f. red-eye in flash photography), any obstructions to the reflected beam are seen as a silhouette. A Nikon 8008 SLR with a Kodak DCS 200 digital camera-back is attached to the photo-slit lamp and is used for image capture. The camera-back has a charge coupled device (CCD) and an on-board hard disk for image storage. The camera is used at  $\times 8$  magnification, with an exposure time of  $1/60$  of a second and with its ISO speed set to 200 [2]. Once captured the images are transferred to a i80486 based PC (with windows) for storage. They are stored individually in separate raw format files, 1024 rows by 1536 columns, 8 bits per pixel, so the size of a file is 1.5 MB (1572864 bytes). From the point of view of image processing (with Khoros) it would be beneficial to group different images of the same patient into a single multi-banded image so that successive bands correspond to images captured in successive appointments. This would allow change with time to be more easily analysed.

Images are identified by encoded information in their file and parent directory names. Encoded information includes: the month of the appointment, indicating when the image was captured (encoded into the parent directory name); the type of IOL used; patient sequence number; patient identity. The latter three attributes being encoded into the file name. A suggested improvement to this nomenclature would be to encode all of these parameters into the file name. Such a nomenclature could be denoted by TSSPPPmXX, where: T is the lens type, identified by the letters: a, b or c. SS is the patient sequence

number, where S is a digit 0, ...,9. PPP is the patient id, where P is a lower case alphabetic character, a, ...,z. m is a flag for the month. XX is the appointment month, where X is a digit 0, ...,9.

### 2.3 Description of Imagery

The images can be visualised with either Khoros or the xv utilities. The latter was found to be the most convenient to use, in particular, with the wait option which provides a mechanism for cycling through a sequence of images. To facilitate visualisation a small shell script was written to convert all the raw images into gif format.

The images are close-ups ( $\times 8$ ) of the IOL region of the eye and have the following facets: (1) a background region with lower grey level that contains some structure; (2) an opening in the anterior capsule (capsulorrhexis), usually approximately circular, but in some cases elliptical or deformed; (3) a pair of lens anchors (haptics) situated near the edge of the IOL; (4) two distinct regions separated by a strong edge within the IOL exposed area. The outer one is the anterior capsule with an incision (usually elliptical) which exposes an inner one - the IOL; (5) At least one small saturated disc-shaped area that is the result of reflections of the source illumination from the front surface of the retina. The anterior capsule has greater opacity than the central exposed lens (IOL) area and is always classed as opacified. The central area contains two different region classes, clear and opacified. Clear regions can either be uniform or can contain irregularities, such as spots, speckles or blemishes. Opacified regions contain either fibrous stands, surface folds, fibrous cellular growth or cellular membrane growth. Fibrous cellular growth has sharp, straight edges and spindle-shaped protrusions (see Figure 1). Regions with membrane cellular growth have curved boundaries, are sometimes globular in appearance and can contain islands of clear especially near the boundaries (see Figure 2). For segmentation four region classes: clear, opacified, background and saturated are therefore required to be identified automatically. Note that it is particularly important to discriminate between clear and opacified regions since it is possible to separate out the background region interactively. The results of a systematic study of the image data is presented in Tables 6, 7 and 8 (see appendix). The symbols used are letter sequences, as defined in Tables 3, 4, 5. The tables provide a detailed description of: (a) which region classes were present, greater than 10% of the interest area, in each of the 169 images. Note, clear regions are implied to exist in all images; (b) information about the shape of the IOL boundary and the shape/orientation of the incision; (c) the exposure, observed quality and other attributes of the imagery. The area of interest is the IOL exposed area that is bounded by the anterior capsule.

### 2.4 Visual Classification of Image Regions

It is easy for the non-expert to distinguish the saturated and background regions from all other region classes. However, it is difficult for the non-expert to distinguish between all types of opacified regions and clear ones. The expertise

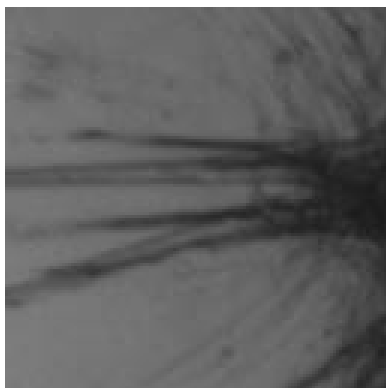


Figure 1: Example of fibrous opacification

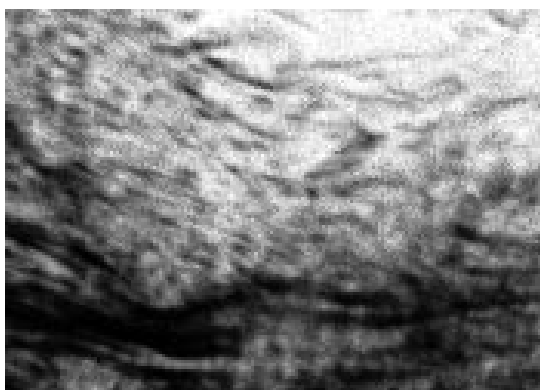


Figure 2: Example of membrane cellular opacification (histogram equalised)

of the Clinician was called upon to help with this. A script was developed that automatically converted the raw format images into postscript format using a special conversion utility (dis). Hard copies of the images were then produced and presented to the Clinician who drew outlines to indicate the opacified regions. The images marked by the Clinician are indicated by the symbol “An” (see tables)

### 3 ANALYSIS OF THE IMAGERY

A wide ranging investigation was undertaken embracing: the available software tools, image noise, statistical properties of the images, textural properties, the class of feature extractors and experiments to evaluate their performance. This was divided into a number of steps as follows: (a) assessment of the software tools for image visualisation, analysis and processing; (b) establishment of a reference set of images; (c) investigation of the noise content of the images; (d) assessment of the general statistical properties of: (i) the full-sized images and (ii) sub-images of the region classes; (e) characterisation of texture and the differences between the different region classes; (f) the proposal of a set of candidate feature extractors; (g) assessment each of the candidates and an evaluation of their performance experimentally. From these results a set of “orthogonal” (in the sense of measuring independent properties) feature extractors were selected to create a feature space. A pattern analyser could then be applied to data points in this space to derive a decision boundary for classification of the different region classes (see later).

#### 3.1 Assessment of Software Tools

It was critically important to have an understanding of the tools available for image processing and visualisation, two major toolsets were assessed as listed below:

##### **xv**

xv is an interactive image display tool for the X windows system, it allows some rudimentary manipulation of imagery and has facilities for converting between many different image formats.

##### **Khoros 1**

Khoros is a comprehensive image analysis/image processing software package consisting of some 255 algorithms. Most of these algorithms are multi-functional and will apply a family of different operators on an image. Khoros uses the viff image format as a standard for all internal operations [4]. The viff format has been designed for 1D and 2D image processing and 3D image visualisation applications. A viff image has a 1024 byte header that describes the file attributes, data storage scheme, the spatial location of pixels and the colour space model [4]. Khoros has been designed to support three levels of user interface: (1)

interactively - using the Cantata visual programming environment; (2) at the UNIX shell level; (3) at the C (or Fortran) programming level.

All of these programming interfaces were investigated. Cantata was used exclusively for the image analysis and for the evaluation of feature extractors. The software tool that was developed for extracting feature vectors (see later) used khoros routines at the UNIX shell level.

### 3.2 Reference Images

Because of the large volume of data a reference set of images were selected for initial consideration. The selection criterion applied was firstly the images must be good quality and secondly that they must have very well defined region classes. The reference set chosen were all month 1 images: a75lev (clear), a47hil (opacified), a33wil (severely opacified and badly deformed).

### 3.3 Noise in Images

It is important to get some measure of the level and nature of the noise present in images because it can adversely affect the performance of an image processing function. Standard analytical techniques for quantifying the noise in an image require either: (a) Knowledge of the scene, for example, knowledge that a particular image sub-region has a uniform grey level. (b) Multiple images of the same scene. Papoulis [5] has proposed a method for estimating the S.N.R. of set of images with additive, zero mean noise that is uncorrelated with the signal. For this data set neither (a) or (b) are available. Although there are images of the same eye, the three b52 (month 3) images, they are at different magnifications. For the purpose of quantifying noise it is suggested that either: (1) multiple images of the same eye be provided; (2) an image of a high definition test card, perhaps the type used for testing an optical system, be provided. To get a rough estimate of the noise level a 50x36 pixel sub-region of the background region of a80fie (month 1), assumed to be uniform, was extracted and the variance in grey level measured. The mean grey level was 21.5 and there was a significant variation of 12 from the mean. This suggested that the images were significantly noisy, but is not a conclusive measure.

### Intensity Ramps

The spatial distribution of intensity (grey level) can give information about the spatial response of the camera system. In particular, the presence of intensity ramps can show whether there is any vignetting. An experiment to test for intensity ramps was carried out with the b02mac (month 1) image. Horizontal and vertical strips were extracted from the background region. The intensity distribution can be considered to be a function of column position,  $x$ , and row position,  $y$ , i.e.  $f(x, y)$ . Figure 3 shows the spatial variation (with column position) of intensity for an horizontal sub-image extract of the background region with bounding coordinates from (16,992) to (1263,1007). The horizontal variation in intensity for four successive rows: i.e.  $f(x, 992)$ ,  $f(x, 993)$ ,  $f(x, 994)$ ,  $f(x, 995)$  for  $16 \leq x \leq 1263$  is shown. Analysis of a  $704 \times 16$  vertical sub-region

## Horizontal Intensity Ramps

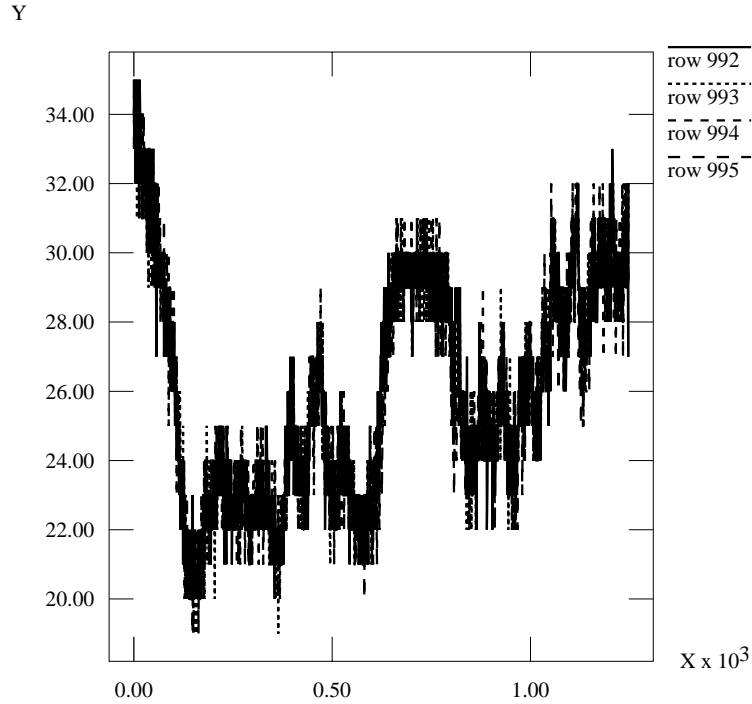


Figure 3: Spatial intensity variation of a horizontal sub-region extracted from the background of b02mac (month 1)

showed similar results. It is clear from the graph that there is no simple linear spatial variation in intensity with position.

### Focusing Errors

The b52ful (month 3) image provides a good illustration of membrane opacification. So two further images of 10 times ( $\times 10$ ) and sixteen times ( $\times 16$ ) magnification have been captured and provide close-ups of this artifact. In particular, the  $\times 16$  image appeared to suffer from a focusing error. However, the increase in magnification results in a decrease the depth of field. It was also observed that the camera appeared to be focussed on the anterior lens surface while the posterior surface, the region of interest, appeared to be out of focus.

### 3.4 Locating the Area of Interest

It was originally proposed that a circular Hough Transform in combination with a flexible snake could be used to detect the boundary of the IOL. However, it can be seen from the tables and from the image in figure 4 that, in some cases, the boundary can be significantly deformed from a circle. So if this approach were to be adopted errors would occur due to these deformities. It was therefore decided to target the segmentation on full-sized images despite the additional computational overhead.

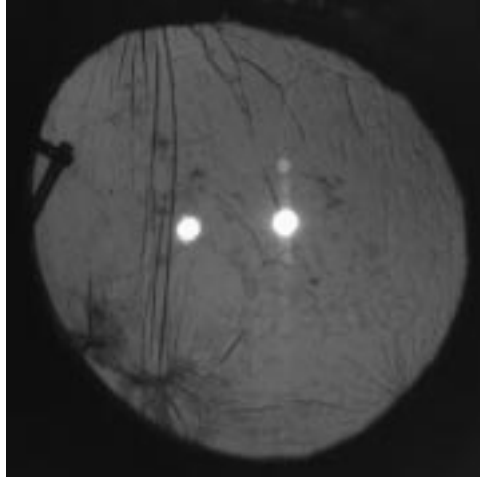


Figure 4: Illustration of the deformed shape of the boundary b90nou (month 1)

### 3.5 General Statistical Properties of the Images

A general measure of grey level variation can be gained by examining the shape of the grey level histogram. Histograms indicate the relative occurrence of different grey levels over an image. A histogram,  $H(f)$ , of an image,  $I$ , is the number of pixels with intensity,  $f$ , defined by:

$$H(f) = \sum_{(i,j) \in I} \delta(f; f(i, j)) \quad (1)$$

where

$$\delta(f; f(i, j)) = \begin{cases} 1, & f = f(i, j) \\ 0, & f \neq f(i, j) \end{cases} \quad (2)$$

Shown in the figures 5, 6, 7 are the histograms of the reference images (produced with Khoros vhssee and xprism2). The histogram of the clear eye image (a75lev month 1) shows a large primary peak centred at 28 (approximately) and a spread between 20 and 40 (approximately). There is a much smaller secondary peak centred at 55 with a wider spread. The histogram of the opacified eye image (a47hil month 1) has a sharp primary peak similar to the clear one. Its secondary peak is centred at 80 and is higher (relative to its primary one) and wider (spread between 70 and 105) when compared with the clear image. The histogram of the second opacified eye image (a33wil month 1) also has the familiar primary peak. Its secondary peak is also higher and wider (spread between 90 and 140) relative to its primary one when compared to the clear image, it is also shifted up the grey scale. Figure 8 shows a histogram of a sub-image extracted from the opacified region of a47hil (month 1). The histograms indicate that there is a greater variation in grey level for the images of opacified eyes when compared with those taken from images of clear ones.

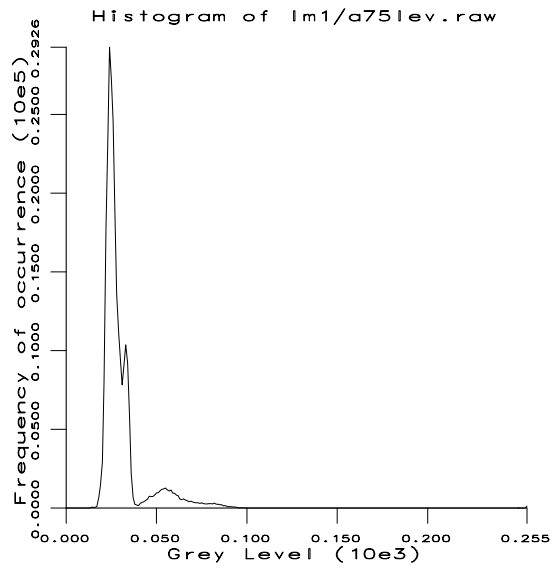


Figure 5: Histogram of a clear eye image

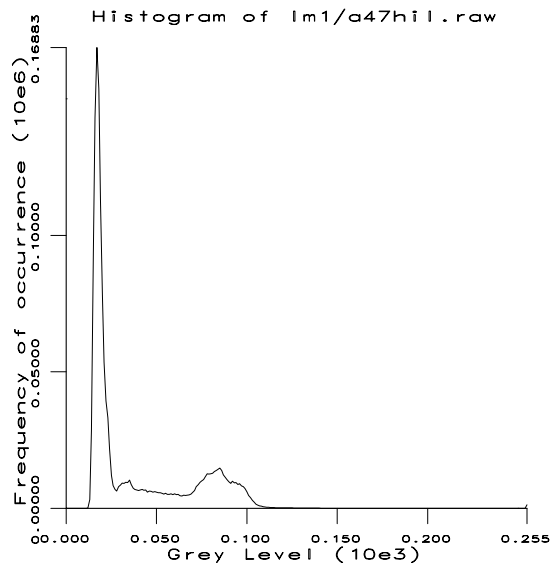


Figure 6: Histogram of an opacified eye image

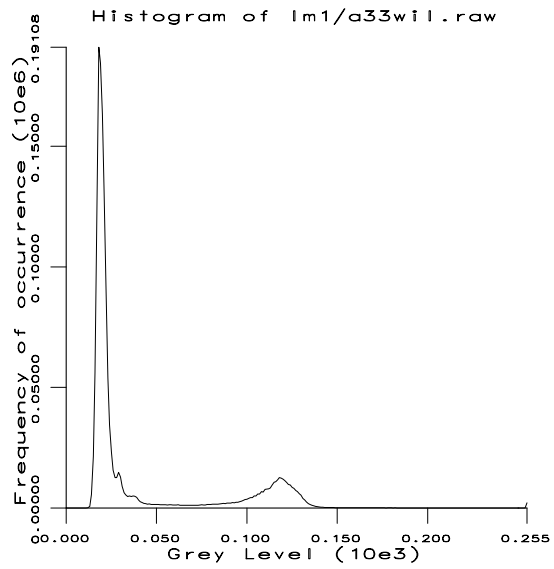


Figure 7: Histogram of a badly opacified eye image

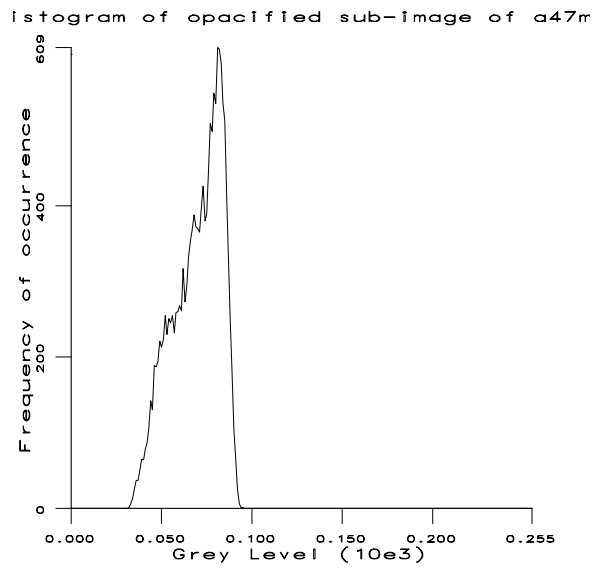


Figure 8: Histogram of an opacified image region

### 3.6 Texture Characterisation of Image Region Classes

A region class has its own distinct texture, so identifying a region amounts to identifying its texture. Texture may be coarse, fine, smooth, granulated, rippled, regular, irregular or linear. Texture can be considered to be constructed from a basic pattern (texel) that is repeated [6] [7]. The distribution of pixels in a texel can be either: periodic, quasi-periodic or random. Natural textures are random and are best characterised statistically [6]. Statistical approaches include: co-occurrence matrices, texture transforms, edge density, band pass filters (texture masks), Fourier spectral analysis, histogram features, mean (where spatial variations in texture are relatively unimportant), variance distribution (where spatial variations are important), random texture fields [6] [7] [8] [9]. In this case, clear regions have a low spatial variation in grey level, however, they are not completely uniform because of spots, speckle, blemishes and other irregularities. In contrast, opacified regions have a higher spatial variation and also a much greater edge density. The cellular growth type of opacification has a coarse, irregular, globular, ripple like texture, with islands of clear regions occurring within it. Saturated regions have a constant grey level of 255 which rapidly decreases outside the boundary. Background regions have a low mean grey level, although, there can be a significant variation.

### 3.7 Feature Extractors

A set of feature extractors for identifying the different textures of different region classes is required. Candidates were first proposed based on the textural properties of region classes. Then they were investigated experimentally. All experiments were carried out with the Cantata visual programming environment (available in Khoros 1). In the first instance a candidate operator was applied to a  $512 \times 512$  pixel sub-region of a47hil (month 1) shown in figure 9. The extracted sub-region contained roughly equal areas of opacified and clear region classes and provided a good initial indicator of the merit of the feature extractor operator. Subsequently the operator was applied to full-sized images. Results were then assessed, if the operator produced a less than ten percent deviation from the boundary between the regions marked by the Clinician then it was adopted.

#### (1) Local Mean

For an image sub-region,  $W$ , containing  $M^2$  pixels with spatial grey level distribution,  $f(i, j)$ , the mean grey level,  $\mu_W$ , is defined as:

$$\mu_W = \frac{1}{M^2} \sum_{(i,j) \in W} f(i, j) \quad (3)$$

The measure,  $\frac{\mu_W}{\mu_I}$  was chosen for feature extraction because it should provide a good criterion for discrimination of the saturated (higher constant mean grey level) and the background regions (lower mean) from other regions. Taking the ratio of local mean and the global mean allows for the multiplicative effect of

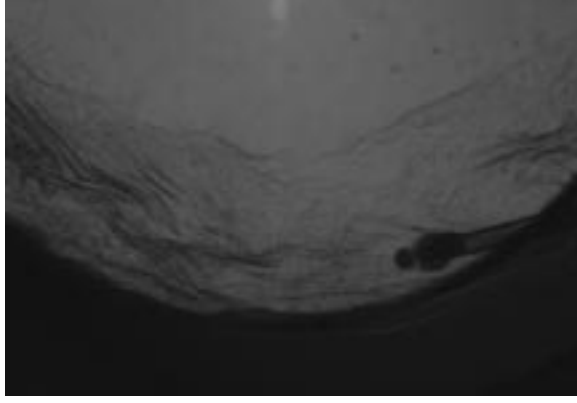


Figure 9: The clear (top) and opacified (centre) regions of a47hil (month 1)

the different exposure levels of different images. A window size of  $7 \times 7$  pixels was selected so as to be consistent with the variance operator (see later).

## (2) Local Variance

The grey level variance,  $\sigma_W^2$ , of an image sub-region,  $W$ , containing  $M^2$  pixels and of mean grey level,  $\mu_W$ , is defined as:

$$\sigma_W^2 = \frac{1}{M^2} \sum_{(i,j) \in W} \{f(i,j) - \mu_W\}^2 \quad (4)$$

From the histogram results and the previous discussion a measure of local spatial grey level variation should provide a good detection criterion for opacified regions. A series of experiments with the reference opacified image, a47hil (month 1), using the Khoros vspatial routine were carried out. The first experiment using a  $3 \times 3$  pixel window, indicated poor discrimination between the two regions. The window size was therefore increased to  $5 \times 5$  pixels. This improved discrimination so the window size was again increased to  $7 \times 7$  pixels. Setting thresholds at grey values of 10 and 50 improved the results still further and provided a very good indicator for opacification see the figure 10. The variance operator was then applied to the other two reference images and showed equally good results. It is likely that the experiments with smaller windows suffered from noise effects and that this could explain their much poorer performance [7]. On the basis of these results it was decided to adopt this operator for feature detection.

## (3) Fractal Dimension

Feature extraction based on fractal dimension [10] has been successfully used in various bio-medical application areas [11] [12].

Fractal geometry is the study of irregular, non-smooth sets. An important property of fractals is that of self similarity, i.e. similarity at different spatial scales. A fractal was originally defined by Mandelbrot [13] to be a set with

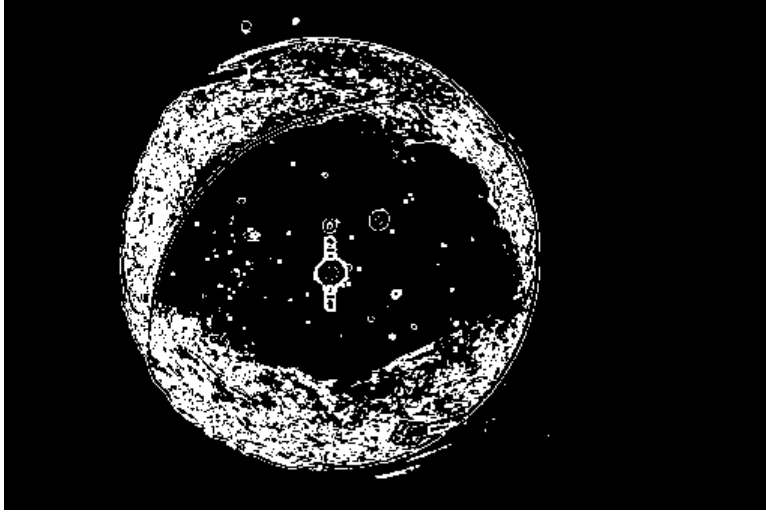


Figure 10: Variance image of a47hil (month 1)

Hausdorff dimension greater than its topological dimension. The Hausdorff dimension of a set  $F$ ,  $dim_H F$ , is the value of  $s$  at which Hausdorff measure,  $\mathcal{H}^s(F)$ , jumps from  $\infty$  to 0, [14]. Where  $\mathcal{H}^s(F)$  is defined by:

$$\mathcal{H}^s(F) = \lim_{\delta \rightarrow 0} \mathcal{H}_\delta^s(F) \quad (5)$$

where  $\mathcal{H}_\delta^s(F)$  is:

$$\mathcal{H}_\delta^s(F) = \inf \left\{ \sum_{i=1}^{\infty} |U_i|^s : \{U_i\} \text{ is a } \delta - \text{cover of } F \right\} \quad (6)$$

and where  $\inf$  is the infimum, the greatest number  $m$ , s.t.  $m \leq x, \forall x \in A$ . Unfortunately, the Hausdorff dimension is difficult to estimate computationally [14], so instead alternative estimates such as box-counting are used. Such an estimate (vpml) is available in Khoros 1. The algorithm uses a number (at least 3) of different windows sizes,  $L$ , to estimate the probability density function,  $P(m, L)$  of a pixel of class  $m$ . A pre-specified set of moment generating functions, of the form:  $\log(M(L)^q)^{\frac{1}{q}}$  are applied to each window and the  $P(m, L)$  distributions calculated. Linear regression is used on the graph of the moment generating function against the log of the window size,  $\log(L)$ , to find the “best fit line”. The slope of the “best fit line” then provides an estimate of the fractal dimension [15]. The routine produces a 3 band image, the first band shows a good discrimination between the clear and opacified regions of a47hil (month 1) see figure 11. Similar results were obtained with the other two images so this operator was adopted as a feature extractor. It is thought that this is because it is a measure of the surface roughness rather than a direct fractal property [10], however, further research is required here.

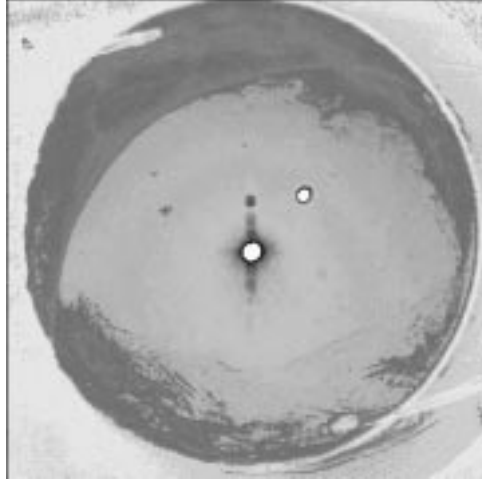


Figure 11: Fractal Dimension Image extracted from a47hil (month 1)

#### (4) Texture Masks

The extraction of features on the basis of local neighbourhood pixel information has been successfully used in a variety of image processing applications of natural scenes [16] [17]. Such an approach has been taken by Laws [18] for the segmentation of natural materials such as: leather, grasses, wool, wood etc... A reported classification accuracy of 87% was achieved (compared to 72% for co-occurrence texture measures). The texture energy is first measured using  $15 \times 15$  pixel masks. Then images are filtered in the spatial domain by convolution with a  $5 \times 5$  Laws texture mask. The masks (kernels) are formed by multiplying any two of a set of five centre-weighted vectors denoted: L5, E5, S5, W5 and R5. A routine (vtexture) is available in Khoros for texture extraction which uses the set of texture kernels derived from the Law metrics [18]. Experiments were performed with all 25 masks using the a47hil (month 1) image. It was observed that the E5L5 mask (horizontal edge detector) and the L5E5 mask (vertical edge detector) produced the best discrimination between the opacified and clear image regions (see figure 12 ). The E5L5 mask is formed by multiplying E5 and L5, where:

$$E5 = (-1 -2 0 2 1) \text{ and } L5 = (1 4 6 4 1)$$

Therefore

$$E5^T L5 = \begin{pmatrix} -1 \\ -2 \\ 0 \\ 2 \\ 1 \end{pmatrix} \begin{pmatrix} 1 & 4 & 6 & 4 & 1 \end{pmatrix} = \begin{pmatrix} -1 & -4 & -6 & -4 & -1 \\ -2 & -8 & -12 & -8 & -2 \\ 0 & 0 & 0 & 0 & 0 \\ 2 & 8 & 12 & 8 & 2 \\ 1 & 4 & 6 & 4 & 1 \end{pmatrix} \quad (7)$$

Note, there was some doubt about the reliability of the vtexture routine, a bug was discovered: if all of the texture mask command line flags are not explicitly included then a 2 band image is produced in error. The first band image is totally white and the second band contains no useful information. It must,

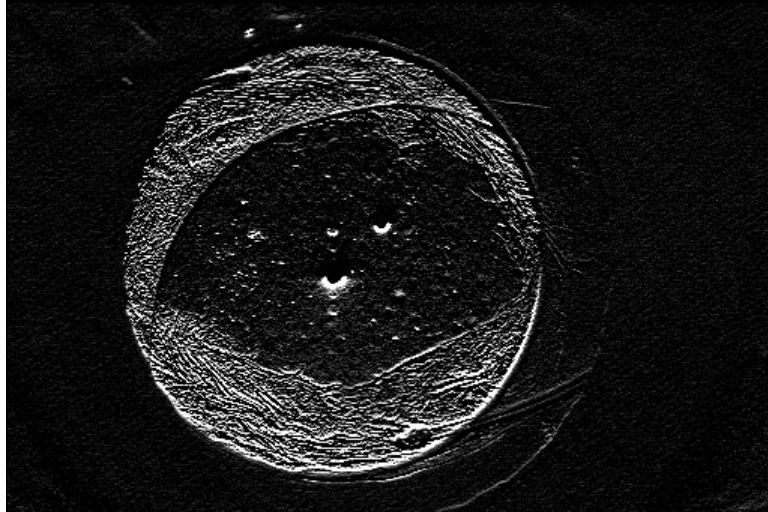


Figure 12: Laws E5L5 texture mask applied to a47hil (month 1)

therefore, be used with all mask flags explicitly set, the ones that are not used must be explicitly set to zero.

### (5) Gradient Analysis

The Laws E5L5 mask has the same form as a gradient operator. It is therefore possible that other operators of the same form might produce better results. Because the cellular growth patterns are anisotropic it was decided that a symmetric gradient operator would be the most suitable. The Roberts gradient operator meets these criteria and was selected for investigation. The operator has the following form:

$$\begin{pmatrix} 0 & 1 \\ -1 & 0 \end{pmatrix} \quad (8)$$

Experiments were carried out with the a47hil (month 1) image. The derivative image produced had a uniform specular appearance and was a poor discriminator between the two region classes. It is likely that the small mask size,  $2 \times 2$  pixels, was particularly affected by noise.

### (6) Fourier Spectral Analysis

The spectral properties of images were investigated by applying a fast Fourier transform (vfft) to the image (see figure 13). The fft requires a square image whose dimensions must be a power of two. The first experiment was aimed at investigating the extent of the spatial frequency spectrum of a clear image a75lev (month 1). An exponential high-pass filter (vhpf) was used with a cut-off frequency of about half the extent of the spectrum. During the course of the experiment it was observed that the largest image that could be transformed was  $512 \times 512$  pixels with the decstation, on another one, with and additional 42 MB of virtual memory, the maximum size was increased to  $1024 \times 1024$  pixels. Since

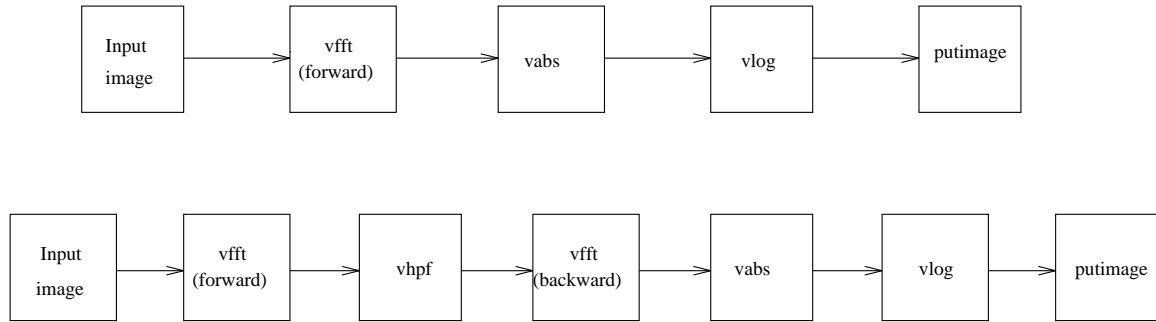


Figure 13: Fourier Transform (above) Fourier Domain Filtering (below)

full-sized,  $1536 \times 1024$  pixel, images could not be transformed (due to limited memory) and because of the image size restrictions it was considered impractical to use Fourier methods for feature extraction. The Fourier transform provides a direct measure of textural coarseness and therefore should provide a good method of discriminating between region classes. A possible way of overcoming the difficulties encountered would be to divide  $1536 \times 1024$  pixel images into a  $3 \times 2$  array of  $512 \times 512$  pixel ones and to transform each of them separately. They could be filtered separately (in Fourier space), inverse transformed and re-assembled as a mosaic.

### (7) Higher Order Moments

Only the mean (first order moment) and variance (second order moment) have been investigated, higher order moments would allow better discrimination between patterns [19]. Khoros (vshape) has 61 different statistical moments including 7 which are invariant to scale, rotation and translation [8] [7]. These moments are probably worth investigating.

### (8) Co-occurrence Matrices

Co-occurrence matrices are based on 2 point statistics, more precisely the joint probability of grey-level distributions within a specified region [7] [6] [20] [8]. They include spatial as well as intensity information and can be a powerful tool for the statistical characterisation of texture. A study into applying them to this problem has been carried out by Paplinski [1]. To avoid duplication and because there was no software available in the Khoros this approach was not investigated.

## 4 THE FEATURE VECTOR EXTRACTOR

From the previous discussion on suitable feature extractor operators, for discriminating the different textures, four in particular were selected: (1) local mean / global mean; (2) local variance; (3) fractal dimension; (4) Laws texture mask; The four different region classes identified were: (1) clear; (2) opacified; (3) background; (4) saturated.

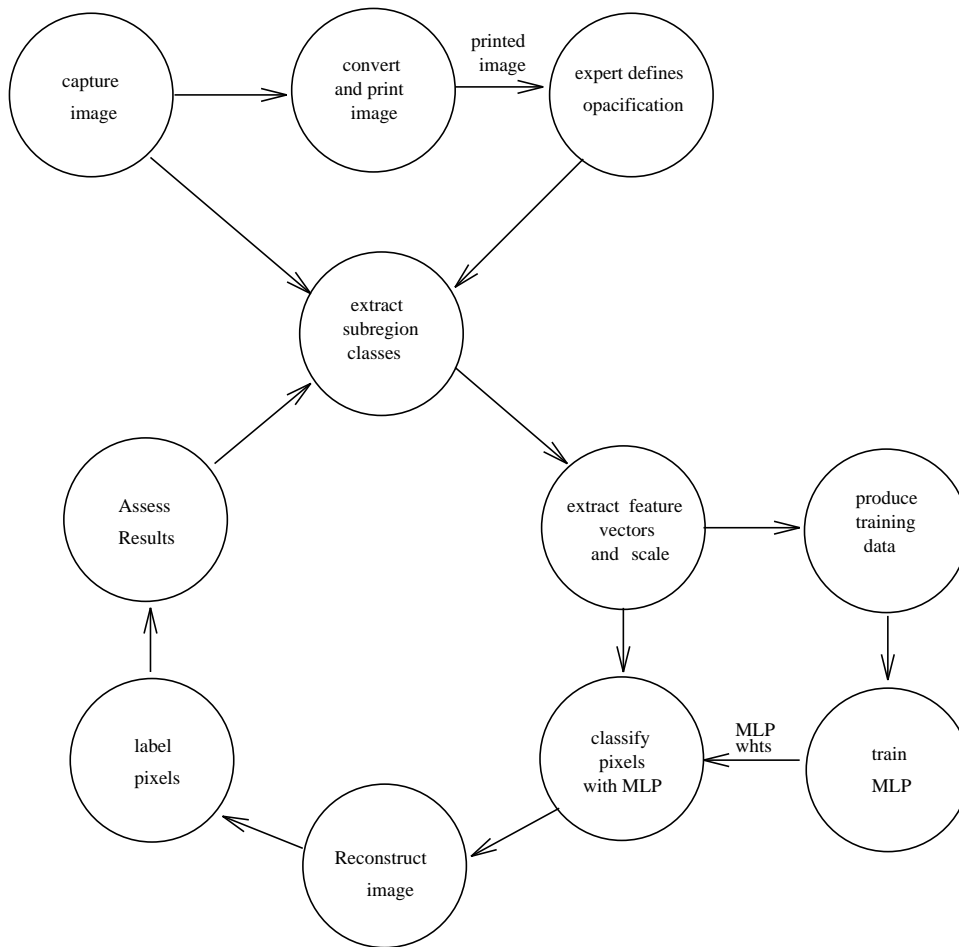


Figure 14: Overall Segmentation Procedure

The problem can, therefore, be re-formulated as one of pattern classification in 4D feature space. One of the most efficient ways to classify patterns is to use a multi-layer perceptron (MLP) neural network [21]. Presented below is a software tool that extracts features using the four feature extractor operators listed above and produces a feature vector that is compatible with that required by an MLP. The tool fits into the overall procedure which is shown in figure 14.

#### 4.1 Software Requirements

The overall aim was to extract a set of features with the above operators from an exemplar set of region classes (viff sub-images) and to generate feature vectors. The feature vectors could then be classified by a MLP pattern classifier (gannet). A tool was required for this purpose that could: (1) deal with changes in the set of exemplar sub-images and their classification. (2) handle variable sized sub-images. (3) provide a way of specifying a common sub-region geometry used for feature extraction; (4) easily incorporate, add or delete feature extractors formulated from Khoros routines; (5) provide the user with some means of

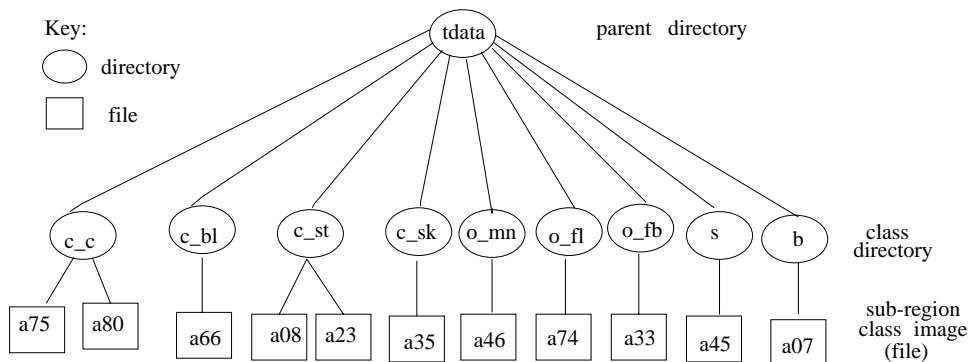


Figure 15: Storage Organisation of training and validation data

specifying a subset of classes, feature extractors and the number of examples produced.

## 4.2 Software Design and Implementation

Initially the C language was considered for implementation. As a result the code generating tools provided by Khoros (composer and ghostwriter) were investigated. However, after consideration of their complexity, the lack of support available and project deadlines it was decided instead to implement using a c-shell script. The c-shell was chosen because: (1) a prototype is required in the first instance; (2) it has C-like arithmetic operators (in contrast to the Bourne shell); (3) UNIX utilities are readily available. Once the algorithm's structure is stable and its usefulness established it could then be re-implemented in a high-level programming language such as C++ or C.

## 4.3 Data Organisation

A set of different region class sub-images are required to be stored and subsequently processed. A simple linear UNIX directory structure was formulated to facilitate this. Each directory containing example sub-images of a particular region class, see figure 15. The database structure can be described by a user-editable file which can be read by the algorithm. The format of the file has one line per sub-image and is prescribed as follows:

```
dir_name file_name class_type_string image_height image_width global_mean
```

## 4.4 The Feature Vector Extractor Algorithm

Given a the set of viff format sub-images and their storage organisation the script performs the following functions: (1) creates a set of feature images (viff format) corresponding to: local\_mean/global\_mean, local variance, fractal dimension, laws texture mask; (2) extracts the central part of each feature image. This is needed because the Khoros routines operate on images with a local patch so the resulting "feature" images have a border, of half the patch size

width containing no useful information, and has to be removed; (3) converts the resulting image to ascii format to facilitate further processing; (4) strips out the grey level field to produce a column vector for each feature; (5) joins the column vectors together to produce a feature vector; (6) calculates the information required for the header and places it at the head of the output file. The figure 16 shows the structure of the algorithm. The algorithm uses the following Khoros routines for image processing:

```
vspatial : extract local statistics (mean and variance) from a viff image.
vpml     : estimate the fractal dimension of a viff image.
vtexture : extract textured image with Laws texture masks
vbandspt1 : separate 0th band of 3 band viff image into a single band image.
vextcent : extract central part of viff image.
vprdata  : convert a viff image to ascii file.
```

Note that the routine for estimating the fractal dimension (vpml) requires a range of, at least three, different moments. It produces a multi-band image, each band corresponding to a different moment. In this case a three band image is produced, however, the 0th band is the only one that is actually used. The band splitting utility (vbandspt1) is used to separate band 0 from the other two to produce a single band image.

### **Format of Feature Vector Output File**

The algorithm generates an ascii format file suitable for processing with a MLP (gannet), with a two line header as follows:

```
total_number_of_features total_of_classes number_of_feature_vectors
begin
```

which is followed by a sequence of lines (one per pixel) with white space separated columns, as follows:

```
feature1 ... featureN class1 ... classM
```

### **Validation of Feature Vectors**

Column vectors representing features can be derived from a feature vector by extracting the appropriate column (using awk). These can be transformed into images by converting the ascii into viff format (ascii2viff). Comparing the resultant images with those generated directly with Khoros (in Cantata) can provide a useful check.

## **5 FEATURE CLASSIFICATION**

Once extracted, feature vectors (patterns) require classification this was done with a multi-layer perceptron (MLP) back-propagation neural network [22]. Classification by MLP is a two stage process. In the first “training” stage input patterns are represented as points in a feature space and a decision surface is

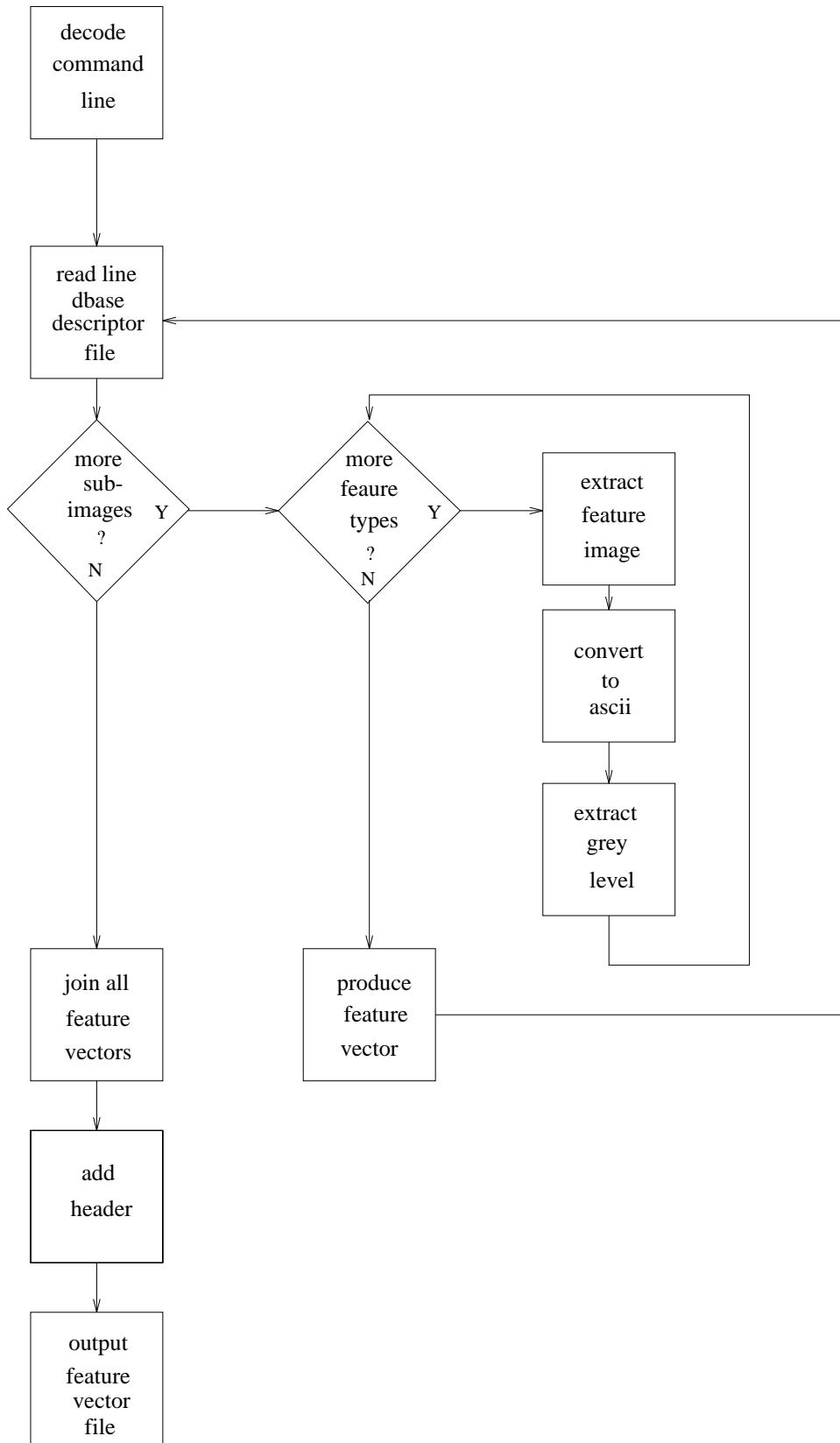


Figure 16: Feature vector extractor control sequence

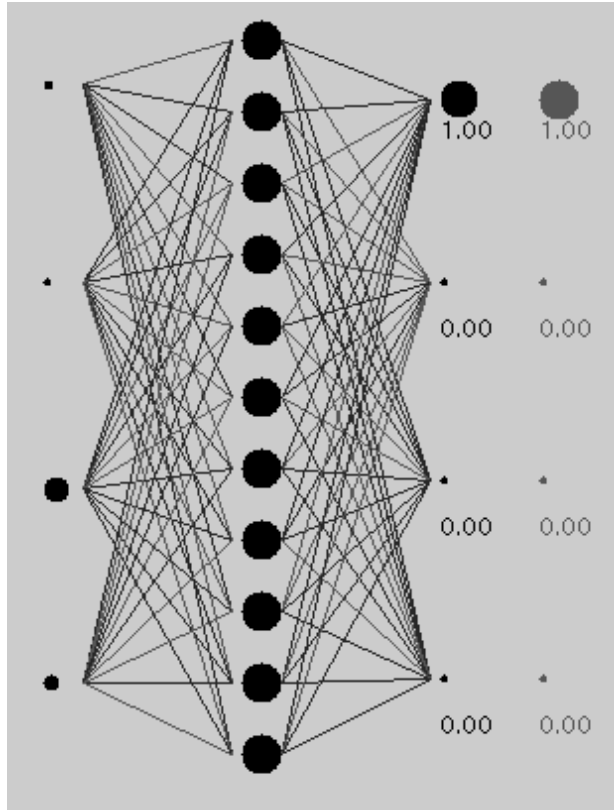


Figure 17: MLP Architecture

calculated from the distributions of the different classes. In the second “classification” stage input patterns are classified according to the decision surface determined in training. The MLP architecture consists of a number of interconnected layers, each layer is composed of a group of nodes which are not connected to each other. Layers are organised so that there is one input layer, a variable number of hidden layers, and one output layer [21]. Figure 17 illustrates a single hidden layer architecture. During the training stage data flow cycles alternately forwards (forward pass) and then backwards (backward pass). During the forward pass input patterns are propagated forwards, layer by layer, with the weights kept fixed. During the backward pass weights are adjusted according to an error correction rule. Error signals are derived from the difference between the obtained output patterns and the target patterns and are propagated backwards [22]. The error signal is used to adjust weights and so minimise the error. Once training has been completed the weights are kept fixed. During the classification stage the weights define the decision surface and patterns are classified according to their relative positions to it.

## 5.1 Training and Validation Data Sets

The training set was chosen to reflect the diversity of texels present for each region class. For example, for clear regions, sub-images were extracted that

contained: areas that were uniformly clear, areas that had spots, areas that had speckle and areas that had blemishes. A similar strategy was adopted for the opacified region class. Extracts were taken from 8 different (month 1) images and 3 different (month 3) images, a total of 11 different images (see table 1 below). Example sub-images were extracted from the interior of the distinct regions to avoid complications that might arise by the inclusion of boundaries. The training data set consisted of a  $10 \times 10$  pixel central sub-region from each of the sub-images listed in the table. There were 600 examples (pixels) that were taken from clear image regions; 300 examples that were taken from opacified ones; and 100 examples that were taken from background ones; 100 examples that were taken from saturated ones (see table) making a total of 1100 pixels. For validation sub-images were taken from a single image (b19bri month 3) different to any of the ones used in training (see table 2). Central  $20 \times 20$  pixel sub-regions were extracted from each of the sub-images listed in table 2 were used. There were 800 pixels extracted from two different clear regions, 800 pixels extracted from two different opacified ones and 400 pixels extracted from a background region. The clear and opacified regions were chosen close to their separating boundary so providing a realistic test.

Training Sub-images			
Image id	Class	Co-ordinates (x,y)	
		top left	bottom right
a75lev (month 1)	1000 c_c	(550,650)	(677,777)
a80fie (month 3)	1000 c_c_ue	(460,660)	(587,787)
a66mch (month 1)	1000 c_bl	(760,670)	(887,797)
a08tow (month 3)	1000 c_st	(620,426)	(747,553)
a23osh (month 1)	1000 c_st_t	(450,500)	(577,627)
a35lap (month 1)	1000 c_sk	(670,580)	(797,707)
a33wil (month 1)	0100 o_fb	(965,555)	(1028,618)
a74fis (month 1)	0100 o_fl	(316,536)	(443,663)
a46fis (month 1)	0100 o_mn	(750,230)	(877,357)
a07kin (month 3)	0010 b	(220,100)	(347,227)
a45gha (month 1)	0001 s	(680,483)	(717,520)

Table 1: Sub-images used for training

## 5.2 Experiments with the Pattern Classifier

An MLP with a single hidden layer, as indicated in figure 17, with a sigmoid-like activation function (gannet) was used. Training patterns were “learnt” by error back-propagation with a least mean squared error (LMSE) correction rule. The MLP minimises errors by searching for the path of greatest gradient of descent on the error surface. The MLP implementation uses two thirds of the input patterns for training and one third for an independent validation check. It also supports interactive control over a number of parameters such as the

Validation sub-images extracted from b19bri (month 3)		
Class	Co-ordinates (x,y)	
	top left	bottom right
1000 c_c	(530,600)	(561,631)
1000 c_sk	(520,740)	(551,771)
0100 o_mn	(500,675)	(563,738)
0100 o_cp	(345,250)	(408,313)
0010 b	(611,36)	(674,99)

Table 2: Sub-images used as validation data

number of nodes in the hidden layer and the size of the search window (step size). Once training patterns are loaded and control parameters set training can commence, starting with a random set of weights. A log of the training statistics, the classification matrix (AKA the confusion matrix) and estimates of the training and validation errors is maintained and can be saved to a file. The number of hidden nodes can be incremented and the log of the training statistics examined to help select the optimal number of hidden nodes. Once the architecture has been chosen the next step is find an optimal set of weights. Weights can be selected on the basis of training statistics accumulated over a number of runs. Two major defects with the implementation were observed: (1) weights could not be loaded for classification; (2) although data scaling was provided there is no information on how this was performed or what scaling factors are used (these factors are required during classification). Experiments showed that auto-scaling was required because some of the features, particularly those derived from the Laws texture mask tended to alternate between large positive and negative values. An auto-scalar was therefore required. For this purpose the image scaling routines in Khoros (vconvert and vnormal) were first investigated, but they did not scale between 0 and 1. So a small script (in awk) was developed. The script passes through the data twice. During the first pass the minimum and maximum values of each feature (first four fields) are extracted. During the second pass these fields are scaled, in accordance with the extrema found in the first one, by the following transformation:  $x \mapsto \frac{x-x_{min}}{x_{max}-x_{min}}$ . The script was shown to produce the same results as the auto-scalar in gannet.

### 5.3 Selecting an Architecture and Weights (Training)

For training the 1100 patterns extracted from the training data set were loaded into the MLP. When the default step size (epsilon) was set to 50 convergence was slow, so it was increased to 200 (with all other parameters set to their default values). Although this resulted in some initial instability a much faster convergence rate was observed. The number of nodes in the input and output layers correspond to the number of features and classes and so are both fixed at 4. The number of nodes in the hidden layer was chosen by cycling through 4 to 32 nodes. Each time 3 runs were executed and the training statistics saved to a

file. For each run the classification matrix, training and validation errors were examined. The experiment showed that 11 hidden nodes was the minimum number required to achieve a fully correct classification and low training error (0.2%) and validation error (0.3%). Weights were selected by performing 10 runs with the 4-11-4 architecture and choosing the set that corresponded with the best training statistics, this was fully correct classification, only non-zero entries in the confusion matrix are on the leading diagonal, with a training error of 0.076% and a validation error of 0.079%. For the classification of validation data another implementation (winner) had to be used. Unfortunately this was found to have a different activation function to the former (gannet). This meant that the weights derived from the former implementation could not be used. So training was repeated with the same parameters and achieved similar results. This implementation was then used for the classification of the validation data.

### **The Classifier in Khoros**

As part of the assessment of the Khoros image processing package a localised receptive field pattern classifier (lrfclass) and an associated trainer (lrftrain) were found but not used. The classifier is based on a single layer of self-organising, "localised receptive field" units followed by a single layer perceptron. The single layer of perceptrons use the LMSE or Adaline learning rule.

## **6 RESULTS**

The classification results for the validation data are as follows. For the two clear regions 791 pixels out of 800 (98.87%) were classified correctly with 9 misclassified as opacified. For the two opacified regions all 800 pixels were correctly classified. For background region only 24 (6%) were classified correctly 375 (94%) were misclassified as opacified.

## **7 CONCLUSIONS**

It was not possible to quantify the noise (suspected to be significant) so a robust feature extraction technique was required. The window size used by a feature extractor was found to be a critical factor. If the window size was too small then poor results are produced (thought to be due to the effects of noise). The approach used has the advantage of adaptability, examples of region classes can be defined by a medical expert and the training data adjusted accordingly. The results obtained from the use of a fractal operator suggest that more complete understanding of the cellular growth might be achieved by modelling it with fractals. The classification results should be viewed as preliminary, results for full-sized images are needed. Nevertheless, the classification accuracy for clear and opacified regions is very encouraging and vindicate the approach taken. The poor classification accuracy achieved for the background, although relatively unimportant, is presumed to be a result of the small number of training

examples used for this region. A larger number should substantially improve the background classification accuracy.

## 8 FURTHER WORK

Additional imagery is required so that noise can be quantified. Image reconstruction software needs to be developed so that the classification results can be represented as an image. The training set needs to be extended to include a variety of different background regions. Experiments to classify full-sized imagery need to be carried out. Cross evaluation against the co-occurrence approach might lead to a better set of feature extractors. Research is needed to establish whether there is any genuine fundamental underlying fractal property of the cellular growth. The integration of an MLP into the Khoros environment with a multi-band viff feature image as an interface would be of great utility.

## ACKNOWLEDGEMENTS

Credits are due to the following: J. F. Boyce (Department of Physics, King's College) for the provision of the computer system, general advice and suggestions on the use of a local mean operator; P. Ursell (Department of Ophthalmology, St Thomas's Hospital, London) for the information on the clinical condition and the equipment used for image capture; D. Toulson (KCL, Physics) for the advise on MLP classifier; M. Brinicombe (KCL, Physics) for DIS and system support. Those who have seen little of me during the long summer much of which was spent carrying out the work.

## References

- [1] Paplinski, A. P. and Boyce, J. F. Computational Aspects of Segmentation of a Class of Medical Images Using the Concept of Conjugate Images. In *IEE Proceedings: Vision, Image and Signal Processing*, 1995.
- [2] P. Ursell. Department of Ophthalmology, St Thomas's Hospital, London SE1, Private communication.
- [3] J. J. Kanski. *Clinical Ophthalmology : a systematic approach*. Oxford, 1994.
- [4] D. Argiro and Gage C. Writing Programs/ VIFF Format. Technical report, University of New Mexico, 1991. Volume II, Chapter 1.
- [5] A. Papoulis. *Probability, random variables and stochastic processes*. McGraw-Hill, 1965.
- [6] A. K. Jain. *Fundamentals of digital image processing*. Prentice Hall, 1989.
- [7] R. J Schalkoff. *Digital image processing and computer vision*. Wiley, 1989.
- [8] R. C. Gonzalez and P. Wintz. *Digital Image Processing*. Addison Wesley, 2nd edition, 1987.
- [9] R. M. Haralick *et al.* Textural Features for Image Classification. *IEEE Trans. Sys. Man. Cyber.*, **SMC-3**:610–621, 1973.
- [10] B. B. Chaudhuri and Sarkar N. Texture segmentation using fractal dimension. *IEEE Patt. Anal. Machine Intell.*, **PAMI-17**:72–77, 1995.
- [11] C. Macaulay and B. Palcic. Fractal Texture Features based on Optical-density Surface. *Analytical and Quantitative Cytology and Histology*, **12** :394–398, 1990.
- [12] R. J. C. Wilding *et al.* The use of Fractal Analysis to Reveal Remodelling in the Human Alveolar Bone following the Placement of Dental Implants . *Archives of Oral Biology*, **40**(1):61–72, 1995.
- [13] B. B. Mandelbrot. *The fractal geometry of nature*. W.H.Freeman, 1982.
- [14] K. J. Falconer. *Fractal geometry : mathematical foundations and applications*. Wiley, 1990.
- [15] R. F. Voss. Fractals in Nature: From characterization to simulation. In H.-O. Peitgen and D. Saupe, editors, *The Science of fractal images*, pages 21–70. Springer-Verlag, 1988.
- [16] R.M. Haralick. Statistical and Structural approaches to Texture. *Proc. IEEE*, **67**(5) :786–804, 1979.
- [17] A Rosenfeld. Image Analysis. In M. P. Ekstrom, editor, *Digital image processing techniques*, pages 257–287. Academic, 1984.
- [18] K. I. Laws. Rapid texture identification. *Society of Photo-Optical Instrumentation Engineers (SPIE)*, **238**:376–380, 1980.
- [19] M. K. Hu. Visual Pattern Recognition by Moment Invariants. *Institute of Radio Engineers trans on information theory*, **IT-8**:179, 1962.
- [20] J.F. Haddon and J.F. Boyce. Image segmentation by unifying region and boundary information. *IEEE Patt. Anal. Machine Intell.*, **PAMI-12**:929–948, 1990.
- [21] S. S. Haykin. *Neural networks : a comprehensive foundation*. Macmillan, 1994.
- [22] D. E. Rumelhart *et al.* Learning Internal Representations by Error Propagation. In *Parallel Distributed Processing: Explorations in the Microstructure of Cognition*, chapter 8 (Vol 1). MIT press, 1986.

## APPENDIX

Key to Region Classes	
clear, (c prefix)	opacified, (o prefix)
c: pristine	Mn: Membrane growth
Bl: Blotchy	Fb: Fiberous strands
Sk: Speckle	Fl: Folds
St: Spots	Cp: Anterior Capsule opacified

Table 3: Symbols used identify region classes

Key to Shape Attributes	
IOL Lens shape	incision shape/orientation
Lc: circular	Ic: circular
Le: elliptical	Ie: elliptical
Ld: distorted	Id: deformed
	Ir: rotated

Table 4: Symbols used to identify shapes

Key to Quality and Miscellaneous Attributes		
Image Exposure	Image quality:	Other Attributes
Eu: under exposed	q1: good	rs: retina scratched
Eo: over exposed	q2: not good	An: Annotated (DS)
f: focussing error	q3: very bad	Td: Training data
t: tears present	<b>X</b> : no image data	Vd: validation data

Table 5: Symbols used to identify image quality etc.

Attributes of type <b>A</b> Images		
Image id	Month 1	Month 3
a05pop	Le	Fl Lc q2
a07kin	Le	Mn Ld Id Td
a08tow	Lc	Bl St Lc Id Td
a10vol	Lc	Fb Fl Ie
a11pla	<b>X</b>	Fb Fl Mn Lc Ir
a14bre	Lc	<b>X</b>
a21nou	Lc	Mn Fl Ld Id
a23osh	Td Lc	Fb Mn St Le Id Ir
a26pep	c t Ld Ie	Mn Bl Lc Ie
a28bro	Fb An Td	Mn? Ld Id q2
a33wil	Fb Le	Fb Sk Mn? Ld q2
a35lap	Fl Td Lc	Fb St Lc q1
a36ega	Lc	<b>X</b>
a38sam	Lc	St Mn? Lc Ie q2
a45gha	An Ic Eu Td	Sk Ld Id q2
a46fis	Fb Lc Td	Mn St Lc Ie
a47hil	Fb An Mn Eu Ir	Fb Bl Sk Mn? Le Ie
a49dor	Fb An Mn St Lc q1	Fb Fl Sk Lc Ir
a50cho	Fl Lc q1	Fb Mn Fl Ir
a53vol	c	Fb Mn q1
a57ple	Fl St Mn Ld Eo	Fl Mn Sk Ld Id
a61gre	Fl Eo	Fb Fl Mn Lc Ie
a63pea	Fl Fb Eu	Fb Lc Id t
a66mch	Bl? Lc q1 Td	Bl Mn? Lc q1
a74fis	Fl Fb q2 Td	Fb Fl Lc Ir?
a75lev	c Lc q1 Td	Fb Lc Ie
a80fie	Fl Ld q1	Fl Sk Eo t? Td
a81sae	<b>X</b>	Fb Sk Ld q2
a81sea	Fb Fl Mn Ld	<b>X</b>
a82eel	Fb Fl t Ld Eu q2	Fb Bl Fl Le q2
a86mye	Fl Fb Lc	Mn Fb Lc

Table 6: Type A lens image attributes

Attributes of type <b>B</b> Images		
Image id	Month 1	Month 3
b02mac	c Fb Fl q1	<b>X</b>
b02mca	<b>X</b>	An St rs Lc Id t?
b04ubs	<b>X</b>	Fl Lc Id Eu t
b15sco	Fb St Sk t Le Ie	c Ld Id q1
b18god	Sk q2	St Lc Id q2
b19bri	Sk Mn Fb t Ld Ie	An Mn St Lc Ie t? q2
b20doo	Bl Sk	<b>X</b>
b25dal	Sk Lc Id Eu q2	An Mn St Lc Ie q2
b27por	c Bl Lc Id Eu	Bl St Mn Lc Ie
b30sta	c bl Ld	<b>X</b>
b31sla	Bl Sk Lc Id Eu q2	St Bl Lc Ie q2
b32kar	c Fb Ie Eu q2	Mn Lc Ie q2
b41ala	<b>X</b>	Ld Id Eu q2
b42tol	Bl St Le Id t	St Le Ie
b44pin	c Lc Id t q1	c Lc Ie
b5210x	<b>X</b>	An Mn Bl
b5216x	<b>X</b>	An Mn Fl
b52ful	Fl Bl Mn Eu q2	An Fl Mn Bl Lc Ie
b55new	Mn Le Ie	Mn Lc Ie
b58ora	Mn q1	An Mn Sk rs Lc q1
b59str	q3	Sk Ld Ie q2
b60lak	q3	Sk Ld Ie q2
b65cor	Mn Lc Eo Id	An Mn Lc Ie
b68cam	Bl Mn Lc Eo	Mn Bl Lc Ie
b69gen	Bl t Eu	Lc t q2
b73col	Ld Id t	c Lc Ie
b77ben	Fb Ld Eu q2	Fb Ld q2
b83nis	Sk Ld t Eu	Sk Ld t Eu q2
b87mcc	<b>X</b>	Bl Mn Lc q1
b87mcr	Fl Sk Mn	<b>X</b>
b89kan	Lc Id Eu q2	Bl Lc Ie t f q2
b90nou	Mn Fb Fl Ld Id q1	Mn Ld
b92col	q3	Bl St Ld Ie f q2

Table 7: Type B lens image attributes

Attributes of type C Images		
Image id	Month 1	Month 3
c01bri	<b>X</b>	Sk St Lc Ie q2
c03lap	Bl Lc	Fb Fl St Le rs
c06gui	c Lc	Fb Mn Lc Id q2
c09hum	Lc Id t	Bl St Lc Ic
c12nel	St Bl Lc	St Sk Mn Ld Ic
c13het	Sk Ld Id t	St Mn Ld Id q2
c16fre	St Lc Id t	Fb Sk Lc Ie
c22nix	Bl Lc	Fl Sk Bl
c24mun	Ld Id q3	<b>X</b>
c29mac	Sk Ld Id q2	Lc Ic q3
c34rea	Sk Ld Ie	An Sk Bl Ld Ie
c37bea	Fb St Lc Ie	An Mn Sk Ir Ie Ld Eo q2
c39mor	Fb St Lc Ie	<b>X</b>
c40smi	Fb Lc	An Fb Sk rs Lc Ie
c48ach	c Lc Ie	An Fl t Lc Ic (b lens)
c51big	Bl Le Ie	Fb Sk Lc? Ie
c56tho	Bl Lc Ie	Fb St Bl Lc
c62law	Fb Fl Mn Ld q1	Fb Mn Lc rs Ie q2
c64gon	q3	Ld Id q3
c67osh	Fb Mn Fl Ld Ic	Fb Mn Ld
c70sla	Fb Mn Lc Eu q3	Fb Sk Lc q2
c71con	c Lc Ie Ir q1	Fb St Fl Mn Lc
c72pag	Fl Fb Mn Lc Ie	Fb Fl Lc Ie
c76bea	Fb St Fl Lc q1	Fb St Fl Lc
c78bry	Bl Lc Eu q2	St Lc Ie t
c79ken	Fl Bl q1 Lc	Fb Fl Mn Bl Lc Ie Eo q2
c84ple	Mn Fl Ld Eu q2	Fl Mn Ld Eo
c85god	Fb Fl Lc Eu q2	Mn Lc rs
c88mes	Ld Eu q2	Bl Sk Ld Ie q3

Table 8: Type C lens image attributes